GTA Weld Cracking—Alloy 625 to 304L

304L rich welds and GTAW-P exacerbate an already sensitive hot cracking problem

BY R. A. PATTERSON AND J. O. MILEWSKI

ABSTRACT. Autogenous gas tungsten arc welds joining alloy 625 and 304L stainless steel were found to be susceptible to weld solidification cracking. Utilization of pulsed current GTA welding produced a higher sensitivity to solidification cracks than continuous current welding. Spot Varestraint tests show that the sensitivity of this dissimilar metal combination to cracking exists over the entire range of dilutions while the greatest sensitivity is in 304L stainless steel rich compositions. Auger electron spectroscopy indicates that segregation of sulfur and phosphorous to the interdendritic phase promotes the hot cracking.

Introduction

Dissimilar metal welding often produces difficulties which may not be obvious when evaluating the system from a design viewpoint. One case in point is the design of nuclear fuel elements for the TREAT reactor (Transient Reactor Test Facility operated by the Argonne National Laboratory, Idaho Falls, Idaho). A high temperature-oxidation resistant alloy (Alloy 625—commercially designated Inconel 625A Trademark of the Inco Family of Companies. The equivalent SAE/ASTM unified number is NO6625.) was specified for the fuel rod cladding, while austenitic stainless steel (type 304L) was used for the cladding end caps due to the lower exposure temperature. Initially, this combination did not indicate a major concern from a weldability viewpoint. However, experimentation revealed a significant susceptibility to solidification cracking for autogenous gas tungsten arc (GTA) welds.

Figure 1 shows that over a relatively broad range of weld heat input, pulsed current GTA welds joining Alloy 625 to 304L exhibit severe centerline cracking. Table 1 lists the range of welding variables used to generate the weld heat input versus weld area graph—Fig. 1. Increasing the frequency of weld current pulsation to nearly 10 Hz tended to decrease the cracking susceptibility which was observed as a qualitative decrease in both the number and length of cracks within a 10 cm (3.9 in.) linear weld. At high pulsation frequencies (~ 10

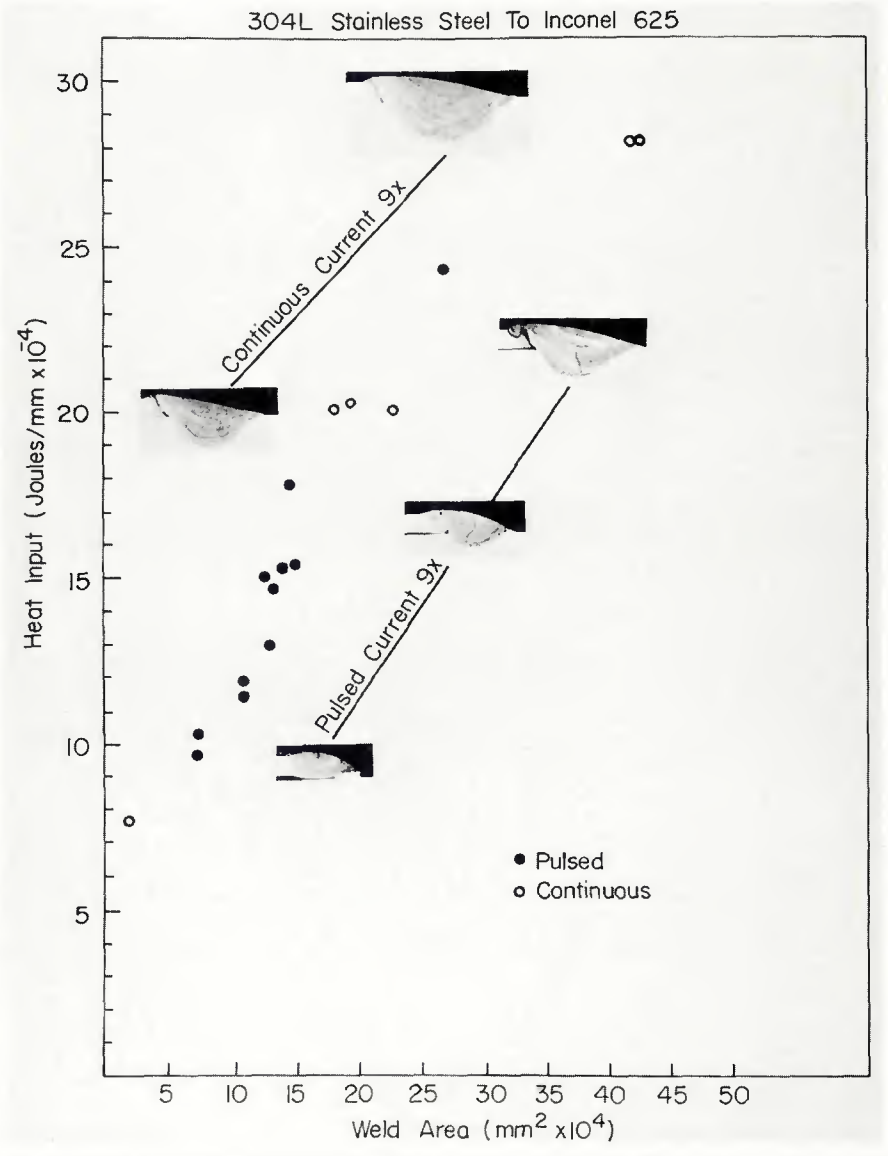

Fig. 1—Graph of weld heat input versus weld cross-sectional area for 304L stainless steel to Alloy 625 gas tungsten arc welds. Note that the pulsed current GTA weld photomicrographs exhibit pronounced centerline cracking

R. A. PATTERSON AND J. O. MILEWSKI are with Los Alamos National Laboratory, Los Alamos, N. Mex.

Table 1—Welding Variable Range Used to Produce Heat Input Versus Weld Area Graph

Parameter	Value Range
Weld Current (A)	30-100
Arc Potential[a] (V)	10-13.5
Weld Speed (mm/s)	1.8-3.6
Pulse Frequency (Hz)	1.5-10
Low Pulse Current (A)	25% of weld current
Pulse Duty Cycle	50%
Torch Gas	Pure Argon
Electrode	1.5 mm dia. W-2% Th
Electrode Tip Geometry	30° included angle to a point

[a]Arc voltage was a dependent variable of the weld current and was set to concur with acceptable welding practice

Hz), the surface appearance of the weld became macroscopically similar to a continuous current weld and as such no effort was made to evaluate the pulsed current welding at higher frequencies. Essentially no cracking susceptibility was observed when utilizing continuous current GTA welding—Fig. 1. This result spawned two questions: Why is pulsed current GTA welding producing an increased cracking susceptibility? What mechanism promotes the cracking in this dissimilar metal combination?

Pulsed current welding has in the past been touted due to reductions in the average heat input and compositional segregation which results in an assumed decrease in weld cracking susceptibility (Refs. 1-3). Reduced average heat input does produce greater uniformity in weld geometry and penetration by reducing the effect of preheat. A second benefit is a reduction in post-weld residual stress (Ref. 1). However, the assumption of reduced compositional segregation is probably not as accurate as stating that the segregated solute is redistributed in a finer second phase due to the higher solidification rates resulting from steeper temperature gradients. Unfortunately, these steeper temperature gradients may increase the susceptibility to cracking through an increase in the stress gradient associated with solidification. Proof of this hypothesis is not presented here, but rather an experimental examination of the cracking mechanism from a weld dilution point of view.

Previous investigators have reported that fully austenitic welds are susceptible to solidification cracking (Refs. 4-8). Robinson and Scott (Ref. 4) reported that cracking in austenitic stainless steels and nickel alloys is promoted by the segregation of S, P, Ti and Nb with a suggested Laves Phase (NbFe) formed in the nickel alloys. Savage, et al. (Ref. 5) reported that segregation of P and S caused hot cracking in Inconel 600. Ogawa, et al. (Ref. 6) reported auger electron spectroscopy (AES) results indicating that P, S and Nb promote cracking in austenitic stainless steel welds and that increased C concentrations appear to counteract the Nb effect. The literature, thus, presents a fairly uniform opinion that segregation of P, S, and Nb in austenitic welds promotes cracking.

The basis for experimentation here was to examine the role of weld metal dilution on the cracking mechanism. An assumed difference in the threshold concentration of elements which promote cracking (S, P, Nb) for either Alloy 625 or 304L is the primary point of discussion. An experiment was designed which allowed weld metal dilution to be varied over a range of nearly 100% 304L to 100% Inconel 625. Cracking susceptibility was monitored using the Spot Varestraint technique since this technique would demonstrate the cracking susceptibility of a single spot weld and perhaps best illustrate the controlling mechanisms in pulsed current GTA welding.

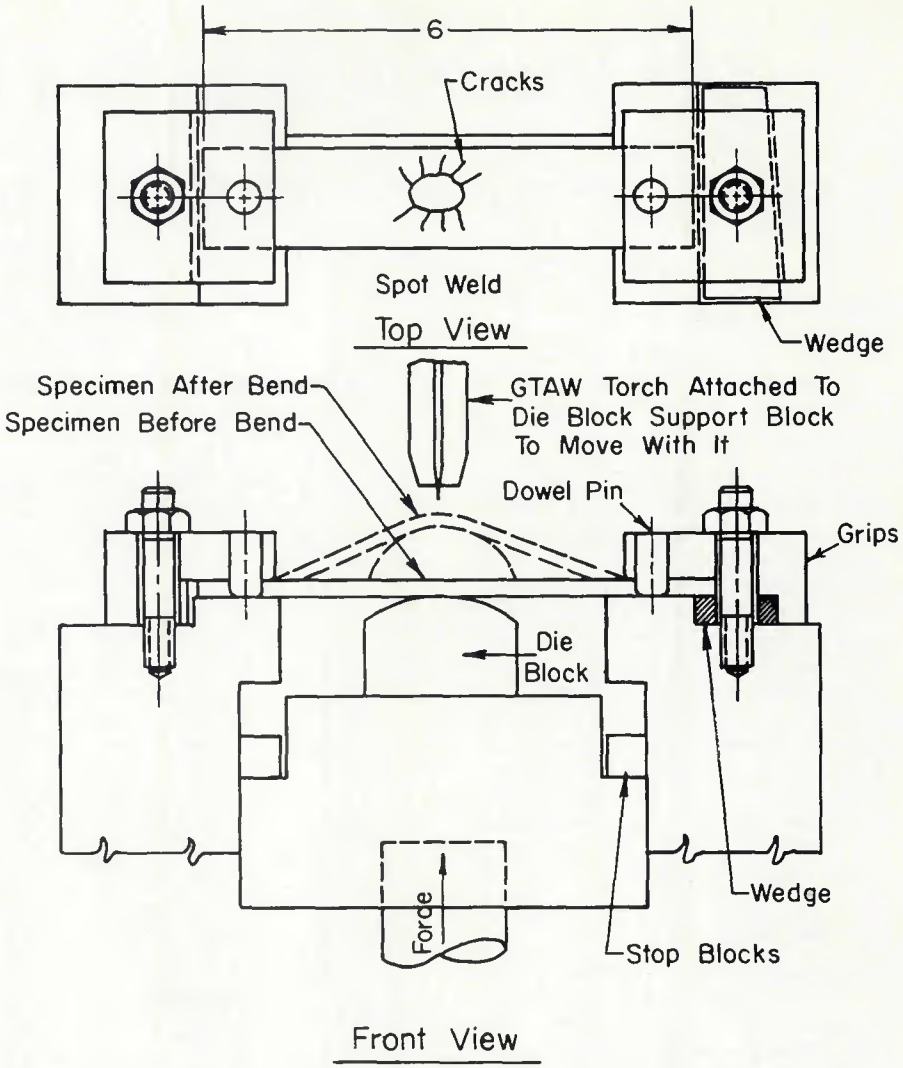

Fig. 2—Schematic of the Spot Varestraint test apparatus showing a weld specimen after bending

Experiment

The Spot Varestraint Test (Refs. 5 and 9) was developed to evaluate the relative hot-cracking sensitivity of base materials. Figure 2 shows schematically the Spot Varestraint Test which incorporates a stationary spot welded specimen that is deformed by a pneumatically driven radius block during solidification. Crack susceptibility is gauged by measuring the total length of weld surface crack versus the amount of augmented strain introduced during solidification. Augmented strain is calculated from the relationship:

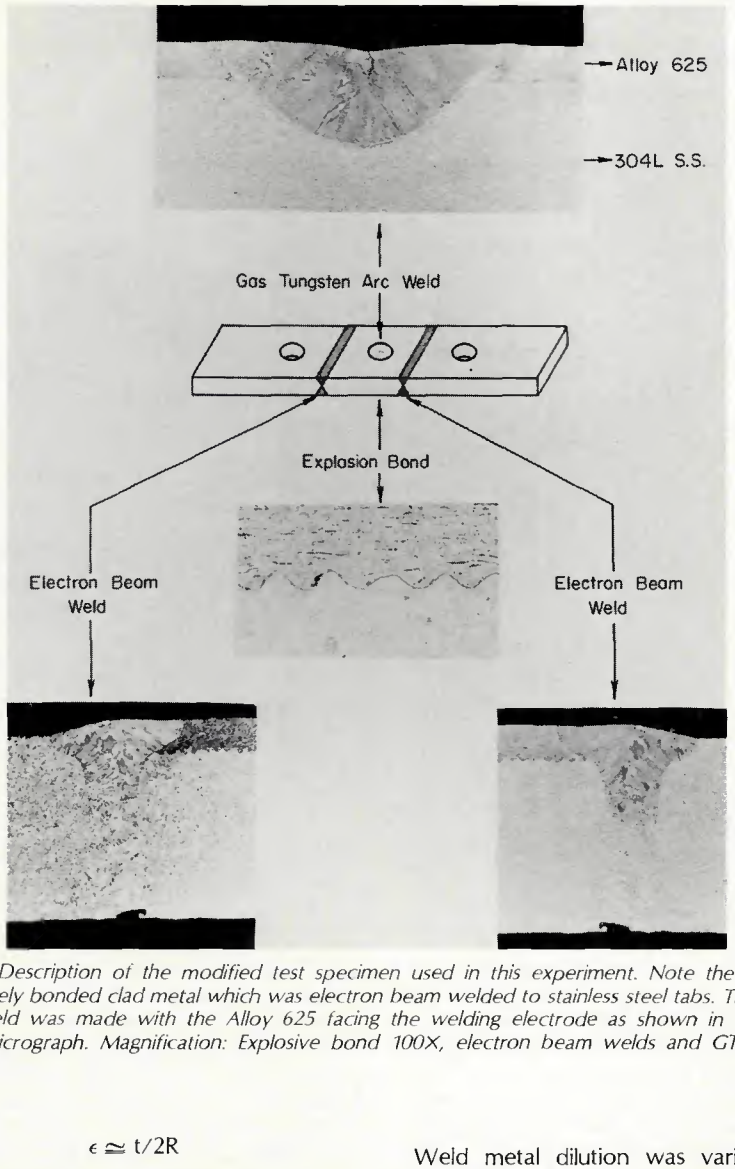

Fig. 3—Description of the modified test specimen used in this experiment. Note the use of explosively bonded clad metal which was electron beam welded to stainless steel tabs. The GTA spot weld was made with the Alloy 625 facing the welding electrode as shown in the top photomicrograph. Magnification: Explosive bond 100X, electron beam welds and GTA weld 15X

$$\epsilon \simeq t/2R$$

where the tangential strain on the specimen top surface, ϵ, is given as a function of specimen thickness, t, and the bending radius, R.

Specimens were cut from sheet stock and measured approximately 20 mm wide by 150 mm long by 3.8 mm thick (0.8 × 5.9 × 0.15 in.). A modified specimen was used for this experiment to allow measurement of crack susceptibility (total length of crack) versus weld metal composition (dilution of Alloy 625 and 304L). Figure 3 shows the specimen which consisted of an explosively bonded clad metal of Alloy 625 to 304L stainless steel (center section), and electron beam welded stainless steel extensions to create the desired 150 mm (5.9 in.) length and yet conserve cladding material. Explosively bonded specimens were used to eliminate the effects of a contact interface between the dissimilar metals and produce specimens which respond in a consistent manner to the augmented strain.

Weld metal dilution was varied by changing the weld penetration to progressively melt greater amounts of 304L, with the Alloy 625 always placed toward the welding arc. Table 2 shows the weld schedule used to vary penetration from approximately 0.64 mm (0.025 in.) (penetration to the Alloy 625-304L interface) to approximately 2.9 mm (0.114 in.) (full penetration). Sequencing of the welding variables was performed with an Amptrak* microprocessor based controller interfaced to a Merrick Engineering Incorporated TXR100 weld power supply.

Weld dilution (defined in this study as the percent of fusion zone which was derived from the 304L) was calculated by volume using the weld centerline cross-sectional area and assuming complete mixing and circumferential weld pool symmetry. Weld pool assymetry did not appear to be prevalent and volume calculations should not introduce significant

**Amptrak® is a registered trademark of Merrick Engineering Incorporated.*

Table 2—Weld Variable Schedule

Level	Time (Seconds)	Current (Amperes)
Prepurge	30	–
Arc Start	1	15
Upslope	1	15 to W.I.[a]
Weld	5	W.I.
Downslope	1	W.I. to 20
Postpurge	30	–

[a]W.I. = Weld current, range 45 to 70 A in 5 A intervals
1. Torch Gas = Pure argon at 35 cfh
2. Arc Length = 1.5 mm
3. Pneumatic Ram Initiation at downslope

errors into the relative dilution versus crack susceptibility determination.

Crack length measurements were performed using macrographs of the weld top surface (10X) as shown in Fig. 4A. Crater cracks were included in the total crack length determination (Fig. 4B), and represent that portion of crack length produced without augmented strain, i.e., cracks resulting from solidification strain. Crack length was normalized with the measured weld cross-sectional area to compensate for changing weld pool volume. This produced a cracking index (CI) equal to the total length of crack divided by the weld area.

Table 3 lists the chemical compositions for each alloy used. Notice that each alloy has a significantly different quantity of P, S, and Nb. Therefore, varying the degree

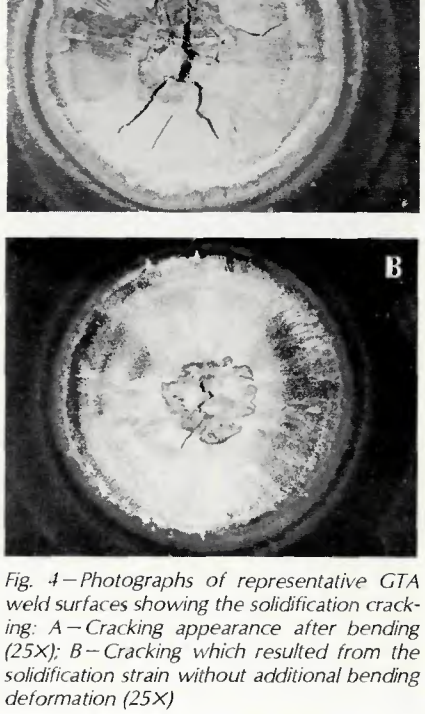

Fig. 4—Photographs of representative GTA weld surfaces showing the solidification cracking: A—Cracking appearance after bending (25X); B—Cracking which resulted from the solidification strain without additional bending deformation (25X)

Table 3—Alloy Compositions (%)

	Fe	Ni	Cr	Mo	Nb	Ta	Mn	Si	C	S	P	Al	Ti	Co
Alloy 625	3.51	60.1	21.5	9.15	3.48	0.044	0.33	0.15	0.024	0.002	0.005	0.20	0.39	0.10
304L ss	Bal.	8.89	18.7	0.3	0.04	0.10	0.66	1.14	0.023	0.019	0.025	0.004	0.0014	0.10

Results of analyses performed at the Los Alamos National Laboratory.

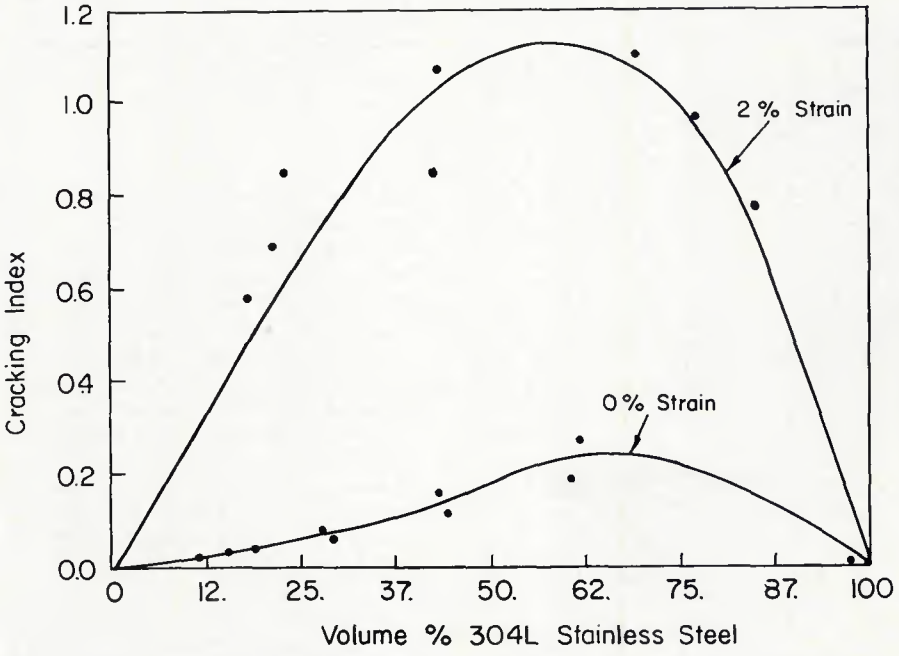

Fig. 5—Graph of cracking index (total length of weld surface crack/weld cross-sectional area) versus calculated weld dilution in volume percent of 304L

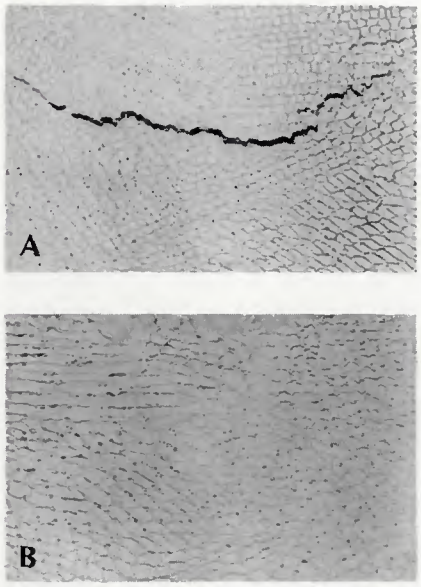

Fig. 6—Transverse cross section photomicrographs of the solidification structures in GTA welds joining 304L and Alloy 625: Top—Photomicrograph of the pulsed current GTA weld microstructure exhibiting a cellular dendritic solidification mode and cracking in the minor phase network (100X); Bottom—Photomicrograph of the continuous current GTA weld exhibiting a similar microstructure to the pulsed current weld (100X)

of intermixing should greatly affect the susceptibility to solidification cracking.

Results

Figure 5 is a graph of cracking index versus weld metal dilution for 0 and 2% augmented strain. Cracking susceptibility resulting from solidification strain (0% augmented strain) appears to be most pronounced in the 304L rich welds. With increased weld strain (2% augmented strain curve), the peak in cracking susceptibility shifts slightly toward 50 percent dilution. These observations indicate that a high solidification cracking susceptibility exists for GTA welds joining 304L and Alloy 625, since measurable cracking occurs with normal solidification strains (0% augmented). Also, the fairly symmetric curve shape (Fig. 5) indicates that compensation for cracking susceptibility is not possible with simple joint design modifications; i.e., decreases in cracking susceptibility require very low dilutions of 304L and, thus, impact effective weld penetration.

Weld metallography revealed that normal cellular dendritic solidification is dominant with crack propagation along interdendritic paths—Fig. 6 (top). Examination of the electron beam welds (Fig. 7),

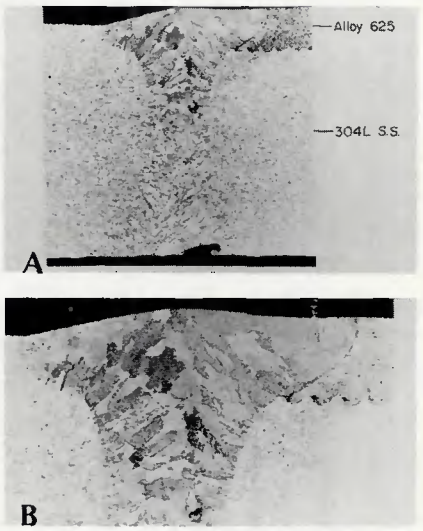

Fig. 7—Photomicrographs of the electron beam welds used to join the explosively bonded clad metal to stainless steel tabs. Note the solidification crack extending from the 304L fusion boundary into the weld fusion zone, indicating increased susceptibility to cracking in 304L rich weld compositions. Magnification: Top 25X, Bottom 50X

further substantiated the observation that cracking is most pronounced in the 304L rich welds. Figure 7 (bottom) shows a typical crack in the EBW which occurs adjacent to the 304L fusion boundary.

Figures 8A and B show typical scanning electron fractographs of the GTA weld cracks resulting from the Spot Varestraint test. Pronounced solidification structures on the crack face are indicative of a weak interdendritic condition at the moment that the augmented strain was introduced.

Borland (Ref. 10) has proposed a generalized theory to explain solidification cracking in terms of segregation and dendrite formation. The theory states that at some point during solidification the primary dendrites become partially interlocked producing a semirigid structure with low melting liquid dispersed among the interlocked dendrites. This structure is not able to accommodate the applied solidification strain and cracking results.

The distribution of the second phase is extremely crucial in determining the cracking susceptibility (Ref. 11). Liquid distribution is controlled by the relative free energies of grain boundaries (solid/solid) and of interphase boundaries (solid/liquid), which are related to the dihe-

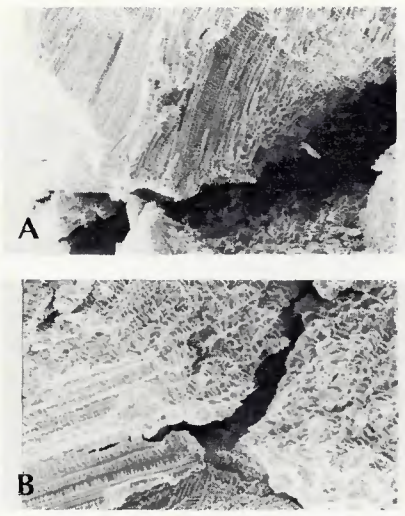

Fig. 8—Scanning electron micrographs of representative crack surfaces showing the pronounced solidification structure appearance which is indicative of interdendritic cracking assisted by a weak near liquid phase. Magnification: Top 250X, Bottom 500X

dral angle as follows:

$$\frac{\delta_{SL}}{\delta_{SS}} = \frac{1}{2\cos\theta/2}$$

where δ_{SL} is the interphase energy, δ_{SS} is the grain-boundary energy and θ is the dihedral angle. As the dihedral angle approaches zero, the liquid forms a continuous film over the grain faces (Ref. 12). This occurs when the ratio δ_{SL}/δ_{SS} is slightly greater than 0.5.

Decohesion of the interdendritic regions is possible when the high stresses resulting from solidification strain are applied directly to a weak and possibly liquid interdendritic phase which is evenly dispersed between the dendrites. Conversely, if the second phase is segmented or confined to grain triple points, the strength of the remaining dendrite boundaries could redistribute the resultant solidification strain and cracking would not occur.

Sulfur, and to a lesser extent phosphorous, have been shown to promote cracking (Refs. 5–8). Cracking has also been reported to be caused by the formation of continuous interdendritic phases, which, due to interfacial tension forces, wet the entire boundary region (Ref. 11). Review of the solidification structure resulting from GTA welds between Alloy 625 and 304L (Fig. 6) reveals that a eutectic-like structure is present with the second phase evenly dispersed around the dendrites.

Auger electron spectroscopic (AES) analysis performed on the fracture surfaces of representative Spot Varestraint specimens indicated that a high degree of S and P segregation had occurred. Alloy constituents which were enriched on the crack surface in descending amounts were S, Nb, P and C while the major alloy constituents, Cr, Ni and Fe, were not significantly different from the bulk weld composition. Niobium enrichments were assumed to result from precipitates since extremely large variations in Nb analysis from one point to the next occurred.

Summary

The results indicate that a significant susceptibility to hot cracking exists in GTA welds joining Alloy 625 and 304L stainless steel. The cracking susceptibility was shown to coincide with the segregation of S, P and perhaps Nb to the interdendritic phase, with S the constituent present in the greatest quantity. These observations are in agreement with the cited literature and in particular the phenomenology proposed by Borland (Ref. 10).

The correlation between cracking index and calculated weld dilution revealed that cracking is more likely in 304L rich welds, which is substantiated by the 0% augmented strain data and the EB weld metallography. These observations indicate that weld joint designs which promote Alloy 625 rich welds would be preferred. This criteria is counterproductive to the present project, since the achievable weld penetration and weld geometry are significantly impacted by reductions in the amount of 304L melted. Also, there is sufficient susceptibility to cracking over the entire weld metal composition range to indicate unacceptable weld reliability for nuclear fuel element fabrication.

Finally, the observation that pulsed current GTA welds exhibited a greater susceptibility to cracking than continuous current GTA welds (Fig. 1) is unexplained. Solidification structures resulting from both techniques appear identical—Fig. 6 (top and bottom). The compositional segregation in pulsed current welding is sufficient to promote cracking, but the segregation occurring in the continuous current welds should not be significantly different. Therefore, the previously postulated increase in solidification stress resulting from steeper temperature gradients and an additional stress imposed by overlapping spot melting events must be sufficient to cause cracking with the pulsed current technique. This is especially true if one spot melting event is only partially solidified during the next melting event.

Conclusions

1. Spot Varestraint tests indicate that gas tungsten arc welds between Alloy 625 and 304L exhibit a high sensitivity to solidification cracking.

2. Auger electron spectroscopy performed on the crack faces indicated that S and P segregation is promoting this cracking sensitivity.

3. Weld metal compositions which are rich in the 304L constituent exhibit the highest susceptibility to cracking as shown most conclusively by the 0% augmented strain curve in Fig. 5.

4. Pulsed current gas tungsten arc welding of 304L to Alloy 625 produces a greater tendency for cracking than the continuous current technique.

5. A modified specimen design has been developed for the Spot Varestraint test which allows the evaluation of dissimilar metal welding.

Acknowledgments

The authors acknowledge the valuable assistance of the following Los Alamos National Laboratory personnel: D. L. Marts for metallography and K. D. Rachocki for AES. Work was performed under the United States Department of Energy contract W7405-Eng 36. We thank Gloria A. Romero for typing the manuscript.

References

1. Ecar, G. M., and Brody, H. D. 1982. Effect of pulsing variables on weld bead size and shape in GTAW of Fe-26% Ni sheets. *Trends in Welding Research in the United States*, ASM, Nov. 16–18, pp. 399–417.

2. Ecar, G. M., Tzaveras, A., Gokhale, A., and Brody, H. D. 1982. Weld pool fluid motion and ripple formation in pulse-current GTAW. *Trends in Welding Research in the United States*, ASM, Nov. 16–18, pp. 419–442.

3. Birman, U. I., and Petrov, A. V. 1971. Influence of the weld metal solidification pattern on hot cracking during pulsed-arc tungsten-electrode welding. *SVAR Proiz*, No. 6. pp. 14–17.

4. Robinson, J. L., and Scott, M. H. 1980. Liquation cracking during the welding of austenitic stainless steels and nickel alloys. *Phil. Trans. R. Soc. Land.*, A 295, pp. 105–117.

5. Savage, W. F., Nippes, E. F., and Goodwin, G. M. 1977. Effect of minor elements on hot-cracking tendencies of Inconel 600. *Welding Journal* 56 (8):245-s to 253-s.

6. Ogawa, T., and Tsunetomi, E. 1982. Hot cracking susceptibility of austenitic stainless steels. *Welding Journal* 61 (3):82-s to 93-s.

7. Linnert, G. E. 1967. Weldability of austenitic stainless steels as affected by residual elements, ASTM STP 418, *American Society for Testing and Materials*, pp. 105–119.

8. Lippold, J. C. 1983. An investigation of heat affected zone hot cracking in alloy 800. *Welding Journal* 62(1):1-s to 11-s.

9. Turner, P. W., and Lundin, C. D. 1970. Effect of iron on the hot cracking of uranium weld metal—part I. *Welding Journal* 49 (12):579-s to 587-s.

10. Borland, J. C., and Younger, R. N. 1960. Some aspects of cracking in welded Cr-Ni austenitic steels. *Brit. Welding J.* 7 (1):22–59.

11. Kammer, P. A., Masubuchi, K., and Monroe, R. E. 1964. Cracking in high-strength steel weldments—a critical review. *DMIC Report 197*, February 7.

12. Smith, C. S. 1948. Grains, phases and interfaces: an interpretation of microstructure. *Trans AIME* 175:15–52.